Biogeotechnics 2 (2024) 100063

Contents lists available at ScienceDirect

Biogeotechnics

journal homepage: www.keaipublishing.com/en/journals/biogeotechnics/

Stress sensitivity of permeability in high-permeability sandstone sealed with microbially-induced calcium carbonate precipitation

Chenpeng Song[a,b,*], Derek Elsworth[b]

[a] Key Laboratory of Hydraulic and Waterway Engineering of the Ministry of Education, Chongqing Jiaotong University, Chongqing 400074, China
[b] Department of Energy and Mineral Engineering and of Geosciences, EMS Energy Institute and G3 Center, Pennsylvania State University, University Park, PA 16802, USA

ARTICLE INFO

Keywords:
Microbially-induced calcium carbonate precipitation (MICP)
High-permeability sandstone
Permeability
Confining pressure
Stress sensitivity of permeability

ABSTRACT

Microbially induced carbonate precipitation (MICP) catalyzed by *S. pasteurii* has attracted considerable attention as a bio-cement that can both strengthen and seal geomaterials. We investigate the stress sensitivity of permeability reduction for the initially high-permeability Berea sandstone (initial permeability ~110 mD) under various durations of MICP-grouting treatment. The results indicate that after 2, 4, 6, 8 and 10 cycles of MICP-grouting, the permeabilities decrease incrementally by 87.9%, 60.9%, 38.8%, 17.3%, and then 5.4% compared to the pre-grouting condition. With increasing the duration of MICP-grouting, the sensitivity of permeability to changes in stress gradually decreases and becomes less hysteretic. This stress sensitivity of permeability is well represented by a power-law relationship with the coefficients representing three contrasting phases: an initial slow reduction, followed by a rapid drop, culminating in an asymptotic response. This variation behavior is closely related to the movement and dislocation of the quartz framework, which is controlled by the intergranular bio-cementation strength. Imaging by scanning electron microscopy (SEM) reveals the evolution of the stress sensitivity to permeability associated with the evolving microstructures after MICP-grouting. The initial precipitates of $CaCO_3$ are dispersed on the surfaces of the quartz framework and occupy the pore space, which is initially limited in controlling and reducing the displacement between particles. As the precipitates continuously accumulate, the intergranular slot-shaped pore spaces are initially bonded by bio-$CaCO_3$, with the bonding strength progressively enhanced with the expanding volume of bio-cementation. At this stage, the intergranular movement and dislocation caused by compaction are reduced, and the stress sensitivity of the permeability is significantly reduced. As these slot-shaped pore spaces are progressively filled by the bio-cement, the movement and dislocation caused by compaction become negligible and thus the stress sensitivity of permeability is minimized.

1. Introduction

The bacterium *Sporosarcina pasteurii (S. pasteurii,* ATCC 11859*)* is a well-known ureolytic bacterium that effectively drives the deposition of calcium carbonate from calcium ions in a urea source (Li, Li, Guo, & Xu, 2023; Zhang, Hu, Wang, & Jiang, 2023). Microbially induced carbonate precipitation (MICP) by *S. pasteurii* has emerged as a fascinating area of research with multiple practical implications (He et al., 2023; Wang et al., 2023a). One area where MICP has shown promise is in geotechnical and geological engineering (Burbank et al., 2013; Wang et al., 2023b). By injecting MICP-reactant solutions (*S. Pasteurii* suspension, $CaCl_2$ and urea solutions) into soil or rock, it is possible to modify their mechanical properties and enhance durability to service and environmental loads (He et al., 2023; Liu et al., 2021; Matsubara, 2021; Salifu et al., 2016; Wu et al., 2019). The bacteria facilitate the precipitation of calcium carbonate within the pore spaces, effectively filling them and increasing the overall strength and stability of geomaterials (Song et al., 2022b; Song et al., 2021) and sealing against flow. Compared to cement-based or chemical grouts, MICP-grouting fluids have a water-like viscosity (approximately 1.5 times that of water) and a very fine entrained particle size (individual bacterial cells present in the MICP-fluids range from 0.5 to 5 μm, with an average length of 2.8 μm), which allows the MICP-fluids to easily penetrate deeply into narrow crevices and pores (Minto et al., 2016; Song et al., 2022a). Furthermore, ureolysis-driven calcium carbonate precipitation by *S. pasteurii* has proven to be highly durable compared to chemical grouts. While chemical grouts typically have a limited lifespan of only ~10–20 years, bio-$CaCO_3$ can provide long-lasting sealing for over 10,000 years (Tobler et al., 2018). This exceptional durability ensures that the structures treated with MICP remain

* Corresponding author.
E-mail address: songchenpeng@163.com (C. Song).

https://doi.org/10.1016/j.bgtech.2023.100063
Received 2 October 2023; Received in revised form 9 November 2023; Accepted 29 November 2023
Available online 21 December 2023

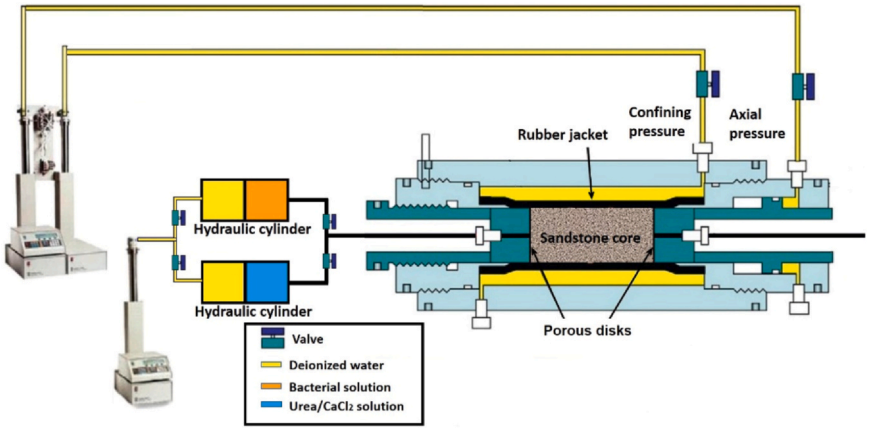

Fig. 1. Schematic of the experimental apparatus for MICP-grouting.

effectively strengthened and sealed for extended periods without requiring frequent maintenance or reapplication.

The evaluation of permeability reduction for MICP-grouted porous and fractured rocks is a crucial aspect of interest. These evaluations allow researchers to compare MICP effectiveness under different geological conditions and provide valuable information for MICP applications such as controlling the transport of contaminants in groundwater, enhancing sweep efficiency in hydrocarbon reservoirs and mitigating leakage in geological carbon storage (GCS) (Cunningham et al., 2009; Daily, 2019; Song et al., 2020; Song & Elsworth, 2020; Wang et al., 2023b). Several laboratory and field studies have observed that multiple cycles of MICP-grouting can lead to more than an order of magnitude reduction in permeability. These studies provide valuable insight into the potential of MICP treatment to improve subsurface engineering applications. However, these studies of permeability reduction in rock fractures and high-permeable rock matrix rarely consider coupling with the stress field (Song et al., 2022a). Permeability in both rock fractures and matrix is typically highly sensitive to changes in effective stress with the evolution of the mechanical behavior of MICP-sealed fractured rock and permeable rock matrix shown to correlate with the filled calcium carbonate content (Song et al., 2022a). Therefore, understanding the linked characteristics of permeability reduction after MICP-grouting under changing in stress conditions is of great significance for MICP-grouting to reduce leakage from carbon sequestration reservoirs, control the transport of contaminants in groundwater and enhance sweep efficiency in hydrocarbon reservoirs.

We investigate the stress sensitivity of permeability for a high-permeability sandstone matrix (initial permeability ~110 mD) to various durations of MICP-grouting. Specifically, Berea sandstone samples are individually treated with either 0, 2, 4, 6, 8 or 10 cycles of MICP-grouting. Subsequently, the permeabilities of each bio-grouted sandstone core are then measured for each 5 MPa increment in confining pressure, loaded from 1 MPa to 41 MPa and then decremented back to the 1 MPa. These observations define exponential and power law relationships describing the stress sensitivity of permeability and inform mechanistic models, unifying these observations across microtextures - allowing the mechanistic characteristic of stress sensitivity to be advanced.

2. Materials and methods

2.1. Preparation of sandstone samples

The sandstone used in this study is from the Devonian in Ohio, USA (Berea sandstone). The sandstone block is cored into cylindrical specimens with a diameter of 25.4 mm and then trimmed to 50.8 mm in length. The mineral composition of the Berea sandstone used in this experiment is mainly composed of quartz (89.6%) with only minor amounts of microcline (6.5%) and kaolinite (3.9%) (Song et al., 2022a). All Berea sandstone cores are cored from the same intact block. We measure the initial porosity and permeability for these Berea sandstone cores and select six cores for which porosity and permeability are closest – and use these as the candidates for MICP-grouting. This will minimize errors and chance factors in the experimental results due to sample discrepancies as much as possible. The porosity and permeability of the Berea sandstone used in this experiment are in the rangesof 19.11% –19.67% and 104.1–116.8 mD, respectively.

2.2. Microbe culture

The urease-producing microorganism utilized in this study was *Sporosarcina Pasteurii*, obtained from the American Type Culture Collection (ATCC 11859, freeze-dried). The growth medium employed NH4-YE as a liquid medium recommended by ATCC (ATCC 1376). The detailed procedure for culturing the bacterial cultures is reported elsewhere (Song et al., 2022a). The bacterial culture solution was collected when the biomass reached OD600 = 1.0.

2.3. Experimental apparatus for MICP-grouting and grouting Strategy

The experimental apparatus for the MICP-grouting is illustrated in Fig. 1. The sandstone core

was placed between stainless steel loading platens with through going flow connections and flow distributors. The core and the platen assembly were isolated from the confining fluid by a fluor elastomer jacket and confined within a 316 L stainless steel core holder capable of applying independent confining and axial stresses. Two high-precision syringe pumps (Teledyne ISCO 260D) with fluid pressures up to 517 bar were used to apply the confining and axial stresses with deionized water as a confining fluid. The sandstone core was loaded to 3.0 MPa in both radial and axial directions throughout the MICP-grouting.

The Berea sandstone samples were individually treated with either 2, 4, 6, 8 or 10 cycles of the MICP-grouting. A single cycle consists of injecting 10 milliliters of bacterial suspension (about twice the pore volume of the sample) and 25 milliliters of the urea-$CaCl_2$ solution [111.0 g/L $CaCl_2$ (1.0 mol/L) and (60.05 g/L urea (1.0 mol/L)] (approximately five pore volumes). The bacterial suspension was first injected into the sample at a flow rate of 0.2 mL/min and subsequently left static (i.e., no flow) for 120 mins to allow the microorganisms to attach to the pore surfaces of the sandstone. The urea-$CaCl_2$ solution was then injected at a flow rate of 0.3 mL/min. Two independent hydraulic cylinders and tubing were used to inject the bacterial suspension and urea/$CaCl_2$ solution to prevent calcium carbonate from settling in the pump and influent flow lines. A syringe pump (Teledyne ISCO 100DX) supplied deionized water to one side of the cylindrical hydraulic piston, expelling a like-volume of bacterial suspension or the urea-$CaCl_2$ solution into the sandstone core. To further homogenize the

distribution of calcium carbonate within the sample, the MICP-grouts were switched across the core during each consecutive grouting cycle (so that the previous injection outlet becomes the new inlet). Between the two successive grouting cycles, one hour was reserved for the preparation of the next grouting cycle and to allow the urea/$CaCl_2$ solution remaining in the pores of the sample to fully react.

2.4. Measurement of porosity, calcium carbonate content and stress-dependent permeability of MICP-treated samples

After the predetermined grouting cycle was completed, the samples were left in the core holder and with no through flow for one hour, then removed from the holder, dried at 80 ℃ for 24 h, and the porosity and calcium carbonate content were assessed. Helium porosimetry was used to gauge the porosity of the sandstone cores after MICP-grouting. The calcium carbonate ($CaCO_3$) content of the MICP-grouted core was determined by measuring the oven-dried mass difference of the cores before and after -grouting and was expressed as the mass of calcium carbonate per unit volume of sandstone (g/cm^3).

After the porosity and calcium carbonate content were determined, the sandstone core was reassembled back into the core holder to evaluate the variation of permeability under different confining pressures. Permeability was measured by injecting distilled water at a constant flow rate. The permeability was evaluated assuming a steady flow and using Darcy's law as,

$$k = \frac{QL\mu}{\Delta pA} \tag{1}$$

where k is the permeability (m^2), Q is the flow rate (m^3/s), L is the core length (m), μ is the dynamic viscosity of the fluid (Pa·s), Δ_P is the pressure difference from the inlet to the outlet (Pa), and A is the cross-sectional area of the sample (m^2).

The sandstone core was loaded to 1.0 MPa in the axial direction throughout the permeability test. The confining pressure begins at 1 MPa, and the permeability is measured at each 5 MPa increment in pressure until the confining pressure reaches 41 MPa. Subsequently, the permeability was measured at each 5 MPa decrement in pressure during unloading until the confining pressure returned to 1 MPa. Each bio-treated sandstone core was subjected to the same experimental schedule.

3. Experimental results and analysis

3.1. Porosity and calcium carbonate content of MICP-treated sandstone cores

Changes in porosity with the progress of MICP-grouting cycles were determined by helium porosimetry. As shown in Fig. 2 (a), the porosity (ϕ) decreases linearly with increasing cycling of bio-treatment. Specifically, after 2, 4, 6, 8 and 10 cycles of MICP-grouting, the porosity of the sandstone cores decreases from 19.11%–19.67% to 17.4%, 15.1%, 13.4%, 11.4% and 10.1%, respectively.

Following the porosity measurements, the mass of precipitated calcium carbonate was determined for various durations of MICP-treatment by measuring the change in oven-dry mass of the sandstone cores before and then after grouting. After 2, 4, 6, 8 and 10 cycles of MICP-grouting, the dry weight of the sandstone cores increased by 1.37 g, 2.76 g, 3.83 g, 4.90 g and 5.86 g, respectively. Fig. 2 (b) illustrates the variations in the mass of calcium carbonate per unit volume of sandstone (g/cm^3), as well as the conversion rate of calcium ions in the urea-Ca^{2+} solution with increasing duration of MICP-grouting. The conversion rate of calcium ions is defined as,

$$\mathrm{Ca^{2+}conversion\ rate}(\%) = \frac{m_n}{M\times n} \times 100\% \tag{2}$$

where m_n represents the mass of precipitated calcium carbonate within the sandstone core after n cycles of MICP-grouting, M represents the maximum theoretical mass of calcium carbonate precipitation that can be synthesized in a single MICP-grouting. That is, 100% of the calcium ions within the urea-Ca^{2+} solution of a single grouting cycle are precipitated into calcium carbonate (up to 2.5 g of calcium carbonate per cycle). When the MICP-grouting transits to 6 cycles, the average conversion rate of calcium ions shows an apparent continuous decline. After 10 grouting cycles, the conversion rate has dropped to 23.1% compared to nearly 28% after only 2 and 4 grouting cycles. It can be inferred that as the precipitated $CaCO_3$ accumulates, the pore space gradually narrows, resulting in an increase in the velocity of the urea-Ca^{2+} solution through the pore throat (since $v \propto 1/\phi$ for constant flow rate experiments). The local microscale velocity is likely to reach the threshold (general Reynold number ≫1), which will lead to the inhibition of bio-$CaCO_3$ precipitation (Wolgemuth, 2008). In this condition, higher local velocities will cause the shear velocity at the pore surfaces to exceed the actual settling velocity of calcium carbonate flocs. According to the conventional theory of particle entrainment, all flocs will be entrained (Mountassir et al., 2014). Furthermore, a higher shear rate at the pore surfaces will also cause the bacteria attached to the pore surfaces to be detached by shear and therefore unable to precipitate (Song et al., 2020, 2019).

3.2. Stress sensitivity of permeability

The sandstone core was loaded to 1.0 MPa in the axial direction throughout the permeability test. The confining pressure began at 1 MPa, and the permeability was measured for every 5 MPa increase until the confining pressure increased to 41 MPa. Subsequently, the permeability was measured at each 5 MPa reduction (unloading) until

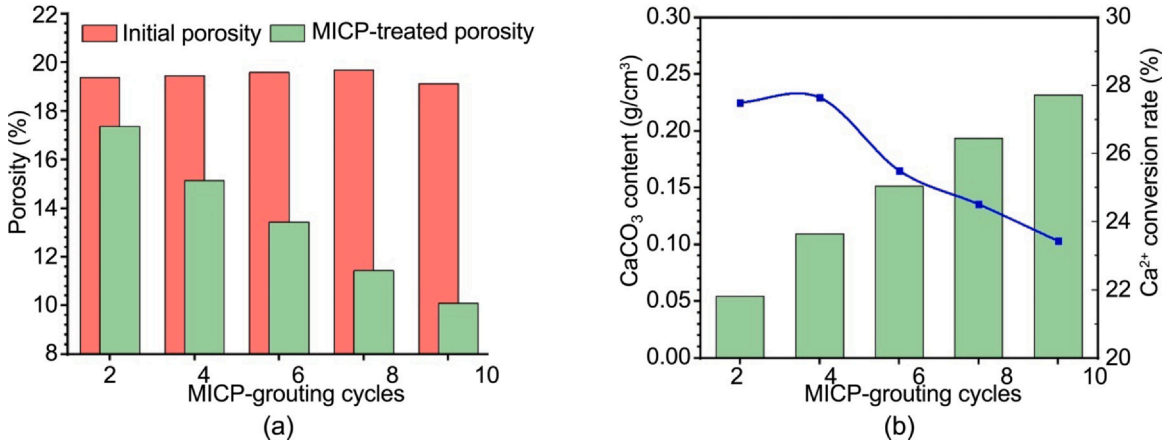

Fig. 2. Variation in (a) porosity, (b) $CaCO_3$ content (g/cm^3) and average Ca^{2+} conversion rate.

the confining pressure was reduced back to 1 MPa in reverse order. Fig. 3(a) shows the measured permeabilities for these sandstone cores after 0, 2, 4, 6, 8 and 10 cycles of MICP-grouting. Comparing the permeabilities relative to the initial confining pressure (1 MPa), the permeability decreases from 104.1 to 116.8 millidarcy (mD) to 91.5 mD, 66.2 mD, 44.4 mD, 19.1 mD and 6.3 mD after 2, 4, 6, 8 and 10 cycles of MICP-grouting. The permeability for the untreated sandstone (0-cycle grouting) is most sensitive to changes in the confining pressure, especially at low confining pressures (0–15 MPa). As the number of grouting cycles increases, the stress sensitivity of the permeability gradually decreases. We further compare the normalized stress-dependent permeability with increasing grouting cycles by normalizing relative to the initial permeability (permeability at 1 MPa) (Fig. 3(b)).

As shown in Fig. 3(b), the permeability shows an exponential decrease then recoveries with the loading then unloading. The stress sensitivity of permeability is at low confining stresses (0–15 MPa), while the stress sensitivity is significantly reduced beyond 15 MPa. The response of permeability to the changes in confining pressure tends to moderate with the increase in grouting cycles. Specifically, the permeability reduction is most significant in the untreated sample when the confining pressure is loaded from 1 MPa to 41 MPa, with a decline of 55%. As the number of cycles/duration of MICP-grouting increases, the amplitude of the decrease in permeability gradually mutes as the confining pressure increases. After ten cycles of MICP-grouting, the permeability at 41 MPa only drops 16% relative to that at the initial confining pressure (1 MPa). In addition, the unloading permeabilities are consistently lower than those during loading as the compaction is not fully reversible. After loading and then unloading, the permeability of the untreated sandstone returns to only 67% of that before loading.

With increasing the cycles of bio-treatment, the permeability recovery rate after loading then unloading gradually rises. After ten cycles of MICP-grouting, the permeability after loading then unloading cycles returns to 92% of that loading. We borrow the concept of the degree of hysteresis in the soil-water characteristic curve (Lu and Khorshidi, 2015) to quantitatively describe the permeability hysteresis in the loading-unloading process. The local degree of permeability hysteresis D_{Pi} is defined as,

$$D_{Pi} = \frac{(P_{li} - P_{ui})}{P_{mi}} \tag{3}$$

where P_{li} is the permeability with confining press at point i during loading, P_{ui} is the permeability at point i during unloading, P_{mi} is the average permeability at point i between the loading and unloading ($P_{mi} = \frac{P_{li} + P_{ui}}{2}$).

As shown in Fig. 3(c), the hysteresis of permeability is significant in the low confining pressure section, and decreases sharply with the increase of confining pressure until the confining pressure increases to 16 MPa, and then the hysteresis of permeability tends to ease. With the increasing duration of groutings, the hysteresis of permeability is significantly weakened, especially in the low confining pressure.

3.3. Models describing stress sensitivity of permeability

Stress sensitivity, an intrinsic property of porous media, is a crucial factor in the behavior of geomaterials under various loading conditions (Tan et al., 2015). It refers to the inherent ability of porous media to deform and compress as a response to applied stress, leading to a subsequent reduction in permeability (Loret et al., 2002; Neto et al.,

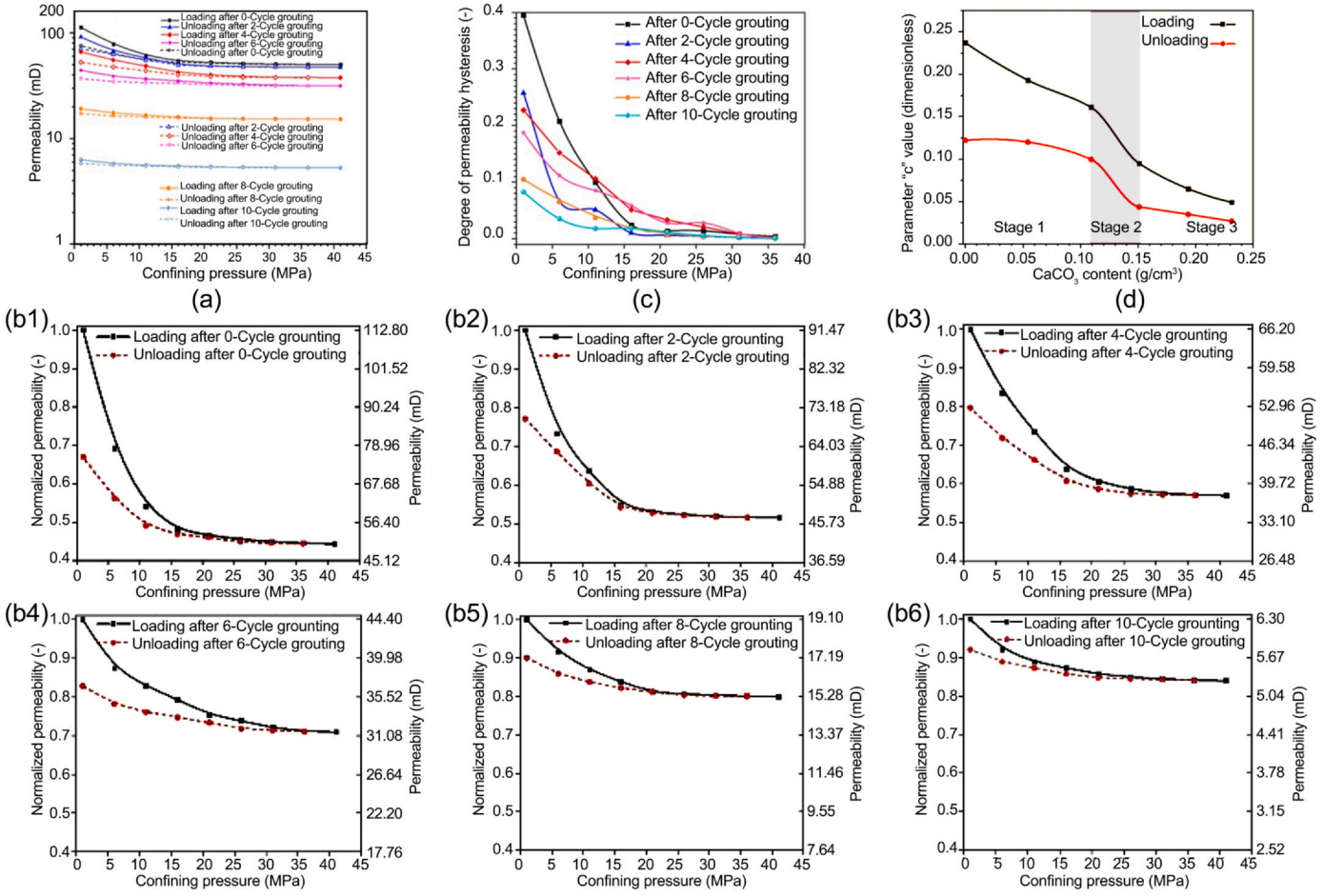

Fig. 3. Variation in (a) stress-dependent permeability, (b) normalized stress-dependent permeability, (c) permeability hysteresis, and (d) correspondence between $CaCO_3$ content and the parameter exponent c in the power law relation for the sensitivity of permeability to stress [(Eq. (5)].

2011). This sensitivity is not limited to specific materials or applications, but is rather a ubiquitous phenomenon observed in both natural and artificial materials, including soils, rocks, and a variety of engineered materials (Khalili & Loret, 2001; Smart et al., 2001).

An exponential relationship suitably describes the stress sensitivity of permeability for sandstones based on the laboratory experiment results(David et al., 1994; Dong et al., 2010; Tan et al., 2015). Such an exponential relationship can be expressed as,

$$k = k_{ref} \exp[-\gamma(p_{eff} - p_{ref})] \quad (4)$$

where k is the permeability of the porous medium at a prescribed effective pressure (m^2); k_{ref} represents the permeability of the porous medium at the reference effective pressure (m^2); γ is the compressibility coefficient (MPa^{-1}), as fitted to experimental data; p_{eff} is the effective pressure (MPa); and p_{ref} is the reference effective pressure (MPa).

The relationship between the effective pressure and rock permeability should follow a power law (Shi & Wang, 1986) as based on the laboratory permeability measurements of Morrow et al. (1984). A power law for describing the stress sensitivity of permeability can be expressed as,

$$k = k_{ref}(p_{eff}/p_{ref})^{-c} \quad (5)$$

where c is a dimensionless parameter fitted to the experimental data.

Parameters γ and c in Eqs. (3) and (4) provide quantitative assessments of the stress sensitivity of permeability. Higher values of γ or c indicate higher stress sensitivity of permeability. Based on the permeability measurement results (Fig. 3(a)), parameters γ and c in Eqs. (3) and (4) are readily determined from curve fitting with the results listed in Table 1. The parameter value γ in the exponential relationship decreases from 0.0226 to 0.00385 (loading) and from 0.0117 to 0.00245 (unloading) as the number of grouting cycles increases. For the power law, the parameter value c decreases from 0.237 to 0.0490 (loading) and from 0.122 to 0.0267 (unloading) with increasing number of cycles of grouting. The coefficient of determination (R^2) for parameters c in the power law is significantly higher than that of parameters γ in the exponential relationship, thus the former more consistently/accurately describes the stress sensitivity of permeability for the sandstone subject to MICP-grouting. Furthermore, we define the correspondence between $CaCO_3$ content within the bio-treated sandstone sample and the magnitude of parameter c in the power law. As shown in Fig. 3(d), with the increase of calcium carbonate content in sandstone, the parameter c for the loading and unloading path gradually reduces, quantifying the decrease in stress sensitivity of permeability. Similarly, the gap of parameter c between the corresponding loading and unloading paths steadily narrows as the precipitated $CaCO_3$ content progressively accumulates. This variation in stress sensitivity with bio-$CaCO_3$ content of Fig. 3(d) is worth further analyzing - since the stress sensitivity after six cycles of grouting (for the pink area in Fig. 3(d)) indicates a steep drop compared to that in the flanking stages 1 and 3. This observed and distinctly different evolutionary trend is likely associated with the calcium carbonate distribution and related cementation within the intergranular spaces of the sandstone. We are conducting microscopic characterizations of the MICP-grouted samples to further explore this posit.

4. Microscopic phenomena and discussion

Scanning electron microscopy (SEM) was employed to investigate the microscopic morphology of microbially induced calcium carbonate and its distribution within the intergranular pore space of sandstone - to elucidate the microscopic processes controlling bio-cementation accumulation and its association with the stress sensitivity of permeability.

4.1. Accumulative process of bio-$CaCO_3$ precipitation in the sandstone framework

We analyzed and contrasted the micro textures of bio-treated sandstone resulting from various durations of MICP-grouting to characterize the accumulation of bio-$CaCO_3$ and the resulting intergranular cementation and clogging. Fig. 4(a)-(f) show SEM images of the original Berea sandstone and after 2, 4, 6, 8 and 10 cycles of MICP-grouting, respectively. The untreated Berea sandstone contains only a limited mass of cementing minerals, as depicted in Fig. 4(a). Sandstone is a clastic sedimentary rock composed of quartz grains bonded together by cementing minerals. The content of cementing minerals significantly affects the mechanical characteristics (strength, modulus) of the sandstone. With the gradual deposition of microbially-mediated calcium carbonate precipitation, the initial deposit of crystalline $CaCO_3$ is dispersed over the surfaces of the quartz grains and occupies the pore space. As the microbially-induced minerals continuously accumulate, the surface coatings expand and thicken. The slot-shaped pore spaces between the quartz grains are the first to be sealed and cemented by the precipitated calcium carbonate. The connection between these slot-shaped pore channels becomes progressively more tortuous, thus resulting in a further decrease in permeability, as well as increasing the bonding strength through ongoing intergranular bio-cementation.

4.2. Evolution of stress sensitivity of permeability after MICP-grouting

David et al. (1994) proposed that the primary mechanisms governing the evolution of rock permeability with confining pressure are microfracture closure, particle rearrangement, and crushing. Three distinct types of permeability evolution induced by mechanical

Table 1
Parameters determined using curve fitting based on the measured permeability of the biotreated sandstones.

Samples with MICP-grouting number	Exponential relationship $k = k_{ref}\exp[-\gamma(p_{eff} - p_{ref})]$		Power law $k = k_{ref}(p_{eff}/p_{ref})^{-c}$	
	Parameter γ (MPa^{-1})		Parameter c (dimensionless)	
	Loading	Unloading	Loading	Unloading
0	0.0226 $R^2 = 0.672$	0.0117 $R^2 = 0.720$	0.237 $R^2 = 0.979$	0.122 $R^2 = 0.978$
2	0.0174 $R^2 = 0.679$	0.124 $R^2 = 0.798$	0.193 $R^2 = 0.979$	0.120 $R^2 = 0.926$
4	0.0154 $R^2 = 0.811$	0.0102 $R^2 = 0.839$	0.161 $R^2 = 0.949$	0.0996 $R^2 = 0.936$
6	0.00838 $R^2 = 0.842$	0.00421 $R^2 = 0.885$	0.0947 $R^2 = 0.977$	0.0435 $R^2 = 0.965$
8	0.00531 $R^2 = 0.747$	0.00321 $R^2 = 0.821$	0.0649 $R^2 = 0.973$	0.0347 $R^2 = 0.980$
10	0.00385 $R^2 = 0.727$	0.00245 $R^2 = 0.812$	0.0490 $R^2 = 0.995$	0.0267 $R^2 = 0.970$

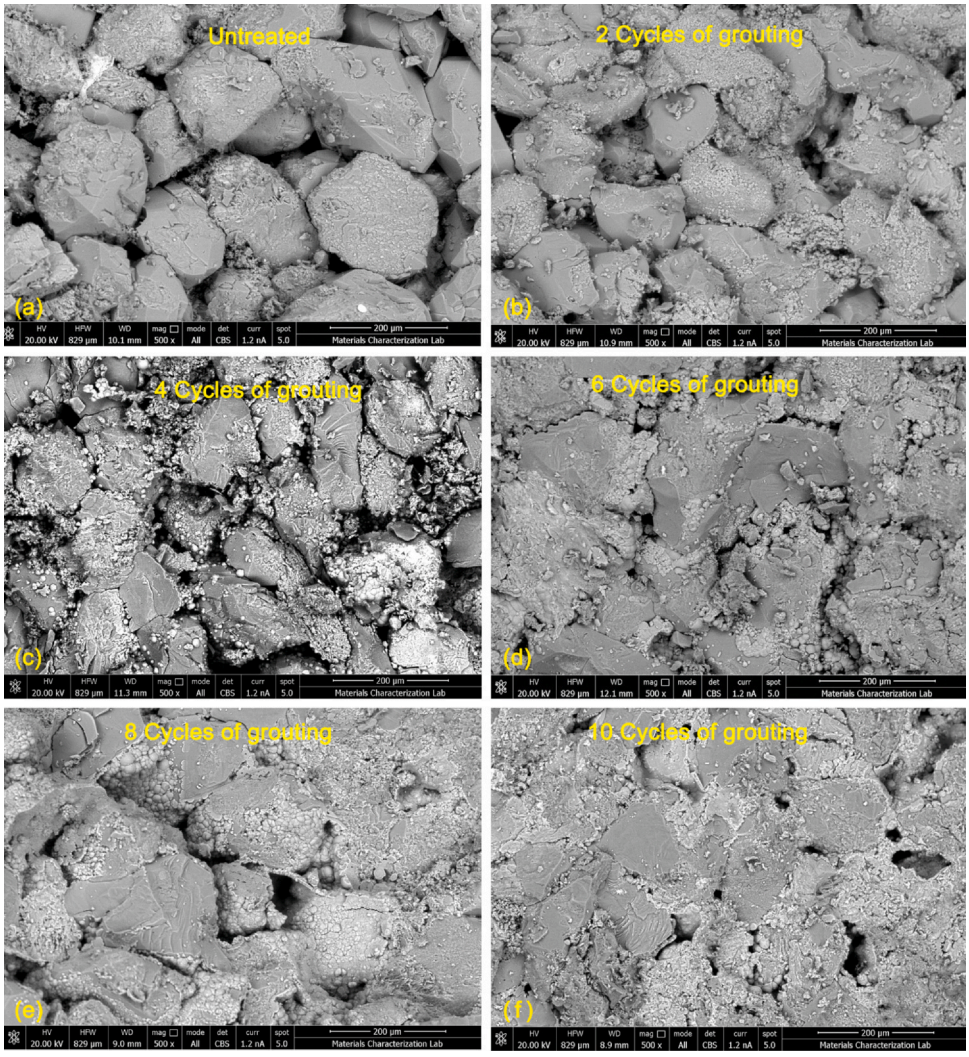

Fig. 4. Textures of bio-$CaCO_3$ accumulation within the high-permeability Berea sandstone.

compaction are proposed in light of this characterization. Type I for low porosity crystalline rock; Type II for porous clastic rock; and Type III, typically for unconsolidated materials. Type II permeability evolution is characteristic of porous clastic rocks, such as sandstones and siltstones, which have a higher porosity due to interconnected pores. This type of permeability evolution is generally sensitive to changes at low stress, where compaction mainly leads to intergranular rearrangement and dislocation. The correspondence between the permeability of bio-treated sandstone cores and the changes in confining pressure is consistent with the Type II permeability evolution. In the initial stage of MICP-grouting, the early precipitates of $CaCO_3$ are dispersed on the surfaces of the quartz grains and occupy the pore voids. The intergranular bonding sites and bonding strength of bio-$CaCO_3$ are relatively limited due to the restricted and isolated accumulation of $CaCO_3$. The precipitated bio-accumulated crystalline $CaCO_3$ moderately reduces and limits the intergranular displacements and dislocations caused by loading – with these displacements and dislocations unlikely to be recovered during unloading. This mechanistic explanation for the initial stages of calcium carbonate accumulation in Stage 1 of Fig. 3(d), suggests that the parameter c, representing stress sensitivity, decreases moderately during the loading process and does not change significantly during the unloading phase. As the precipitated $CaCO_3$ continuously coats the surfaces of the quartz grains, the bonded areas in the slot-shaped voids gradually increase, resulting in a rapid increase in intergranular stiffness with an augmentation of $CaCO_3$ mass. At this stage, the intergranular movement and dislocation caused by compaction are markedly reduced, together with the stress sensitivity of permeability, as in stage 2 of Fig. 3(d). As the slot-shaped voids are almost fully-cemented and filled with the precipitated calcium carbonate, the interparticle bio-bonding strength ultimately plateaus, and the movement and dislocation caused by compaction become minimal. Thus, the stress sensitivity of the permeability decreases with the bio-accumulation of the $CaCO_3$ (Stage 3 in Fig. 3(d)) and the stress sensitivity of the permeability in the loading and unloading paths almost coincides.

The evaluation of permeability reduction for MICP-grouted porous and fractured geomaterials is a crucial aspect of interest. This study provides insight into the correlation characteristics of permeability reduction for porous clastic rocks, such as sandstone, after MICP-grouting under changing in stress conditions. Although the Berea sandstone used in this study is a common candidate for rock experiments, it contains almost no clay minerals and has good water stability. The sandstone selected for this experiment has certain limitations in mineral composition. The presence of clay minerals in the sandstone may affect the macroscopic mechanical behaviors and associated permeability after MICP-grouting. Clearly, this requires further research. In addition, current studies of MICP-grouting for permeability reduction in rock fractures also rarely consider the coupling with the stress field. This will undoubtedly be the focus of our next work.

5. Conclusions

This work investigates the stress sensitivity of permeability in the high-permeability Berea sandstone subject to various durations of MICP-grouting – as representative of other high permeability clastic rocks. Observations for permeability reduction indicate that the permeability significantly declines with increasing durations of MICP-grouting – represented by increasing number of cyclic treatments. The permeability after ten cycles of grouting (the longest treatment) declines from 116.8 mD to 6.3 mD, a reduction of ~95%. The variation in stress sensitivity for permeability with increasing duration of MICP-grouting indicates that the permeability for the untreated sandstone is most sensitive to changes in the confining pressure, especially at low confining pressures (0–15 MPa). As the durations of MICP-grouting increase, the stress-dependent permeabilities in the loading and unloading paths almost coincide and as the strong hysteresis at lower cementation contents disappears.

A power law relation describing the stress dependency of permeability is shown superior to an exponential relationship for this particular high-permeability sandstone sealed with bio-accumulated $CaCO_3$. The exponent, c, in the power law relationship is able to quantitatively evaluate the stress sensitivity of permeability. The variations in the parameter value c with bio-accumulation of $CaCO_3$ represent three contrasting phases of stress sensitivity: an initial slow reduction, followed by a rapid drop in permeability with stress and then asymptotic to minimal sensitivity.

The stress sensitivity of permeability for porous clastic rocks, such as sandstone, is mainly due to intergranular movement and dislocation caused by compaction. Imaging by scanning electron microscopy (SEM) reveals the evolution of the stress sensitivity for permeability associated with evolving microstructures after MICP-grouting. At first application, the initial precipitates of $CaCO_3$ are dispersed on the surfaces of the quartz framework and occupy the pore voids, which is limited in controlling and reducing the displacement between particles. As these precipitates continuously accumulate, the resulting intergranular slot-shaped pore spaces are first bonded by bio-$CaCO_3$, with the bonding strength progressively enhanced with the expanded area of bio-cementation. At this stage, the intergranular movement and dislocation caused by compaction are clearly reduced along with the stress sensitivity of permeability. As these slot-shaped pore spaces are almost fully bio-cemented, the movement and dislocation caused by compaction become very slight, and the stress sensitivity of the permeability is finally minimized.

CRediT authorship contribution statement

Chenpeng Song: Conceptualization, Data curation, Formal analysis, Funding acquisition, Investigation, Visualization, Writing – original draft, Writing – review & editing. **Derek Elsworth:** Conceptualization, Formal analysis, Supervision, Visualization, Writing – review & editing.

Declaration of Competing Interest

The authors declare that they have no known competing financial interests or personal relationships that could have appeared to influence the work reported in this paper.

Acknowledgments

This work was funded by the National Natural Science Foundation of China (Grant No. 51604051) and the Natural Science Foundation of Chongqing (Grant No. CSTB2022NSCQ-MSX0372). DE acknowledges support from the G. Albert Shoemaker endowment. The authors are grateful for this support.

References

Burbank, M., Kavazanjian, E., Weaver, T., Montoya, B. M., Hamdan, N., Bang, S. S., Esnault-Filet, A., Tsesarsky, M., Aydilek, A., Ciurli, S., Tanyu, B., Manning, D. a C., Larrahondo, J., Soga, K., Chu, J., Dejong, J. T., Cheng, X., Kuo, M., Al Qabany, A., Seagren, E. A., Van Paassen, L. A., Renforth, P., Laloui, L., Nelson, D. C., Hata, T., Burns, S., Chen, C. Y., Caslake, L. F., Fauriel, S., Jefferis, S., Santamarina, J. C., Inagaki, Y., Martinez, B., & Palomino, A. (2013). Biogeochemical processes and geotechnical applications: progress, opportunities and challenges. *Géotechnique, 63*, 287–301. https://doi.org/10.1680/geot.SIP13.P.017

Cunningham, A. B., Gerlach, R., Spangler, L., & Mitchell, A. C. (2009). Microbially enhanced geologic containment of sequestered supercritical CO_2. *Energy Procedia, 1*(1), 3245–3252. https://doi.org/10.1016/j.egypro.2009.02.109

Daily, R. L. (2019). A study of bio-mineralization for the application of reducing leakage potential of geologically stored CO_2 *(Doctoral dissertation. Montana State University-Bozeman, College of Engineering)*. https://doi.org/10.1017/CBO9781107415324.004

David, C., Wong, T. F., Zhu, W., & Zhang, J. (1994). Laboratory measurement of compaction-induced permeability change in porous rocks: Implications for the generation and maintenance of pore pressure excess in the crust. *Pure and Applied Geophysics, 143*, 425–456. https://doi.org/10.1007/BF00874337

Dong, J. J., Hsu, J. Y., Wu, W. J., Shimamoto, T., Hung, J. H., Yeh, E. C., Wu, Y. H., & Sone, H. (2010). Stress-dependence of the permeability and porosity of sandstone and shale from TCDP Hole-A. *International Journal of Rock Mechanics and Mining Sciences, 47*, 1141–1157. https://doi.org/10.1016/j.ijrmms.2010.06.019

He, J., Liu, Y., Liu, L., Yan, B., Li, L., Meng, H., Hang, L., Qi, Y., Wu, M., & Gao, Y. (2023). Recent development on optimization of bio-cementation for soil stabilization and wind erosion control. *Biogeotechnics, 1*(3), Article 100022. https://doi.org/10.1016/J.BGTECH.2023.100022

Khalili, N., & Loret, B. (2001). An elasto-plastic model for non-isothermal analysis of flow and deformation in unsaturated porous media: formulation. *International Journal of Solids and Structures, 38*, 8305–8330. https://doi.org/10.1016/S0020-7683(01)00081-6

Li, Y., Li, Y., Guo, Z., & Xu, Q. (2023). Durability of MICP-reinforced calcareous sand in marine environments: Laboratory and field experimental study. *Biogeotechnics, 1*(2), Article 100018. https://doi.org/10.1016/J.BGTECH.2023.100018

Liu, B., Xie, Y. H., Tang, C. S., Pan, X. H., Jiang, N. J., Singh, D. N., Cheng, Y. J., & Shi, B. (2021). Bio-mediated method for improving surface erosion resistance of clayey soils. *Engineering Geology, 293*, Article 106295. https://doi.org/10.1016/j.enggeo.2021.106295

Loret, B., Hueckel, T., & Gajo, A. (2002). Chemo-mechanical coupling in saturated porous media: elastic–plastic behaviour of homoionic expansive clays. *International Journal of Solids and Structures, 39*(10), 2773–2806. https://doi.org/10.1016/S0020-7683(02)00151-8

Lu, N., & Khorshidi, M. (2015). Mechanisms for soil-water retention and hysteresis at high suction range. *Journal of Geotechnical and Geoenvironmental Engineering, 141*(8), Article 04015032. https://doi.org/10.1061/(ASCE)GT.1943-5606.0001325

Matsubara, H. (2021). Stabilisation of weathered limestone surfaces using microbially enhanced calcium carbonate deposition. *Engineering Geology, 284*, Article 106044. https://doi.org/10.1016/j.enggeo.2021.106044

Minto, J. M., MacLachlan, E., El Mountassir, G., & Lunn, R. J. (2016). Rock fracture grouting with microbially induced carbonate precipitation. *Water Resources Research, 52*(11), 8827–8844. https://doi.org/10.1002/2016WR018884

Morrow, C. A., Shi, L. Q., & Byerlee, J. D. (1984). Permeability of fault gouge under confining pressure and shear stress. *Journal of Geophysical Research: Solid Earth, 89*(B5), 3193–3200. https://doi.org/10.1029/JB089iB05p03193

Mountassir, G. E., Lunn, R. J., Moir, H., & MacLachlan, E. (2014). Hydrodynamic coupling in microbially mediated fracture mineralization: Formation of self-organized groundwater flow channels. *Water Resources Research, 50*(1), 1–16. https://doi.org/10.1002/2013WR013578

Neto, L. B., Kotousov, A., & Bedrikovetsky, P. (2011). Elastic properties of porous media in the vicinity of the percolation limit. *Journal of Petroleum Science and Engineering, 78*(2), 328–333. https://doi.org/10.1016/j.petrol.2011.06.026

Salifu, E., MacLachlan, E., Iyer, K. R., Knapp, C. W., & Tarantino, A. (2016). Application of microbially induced calcite precipitation in erosion mitigation and stabilisation of sandy soil foreshore slopes: A preliminary investigation. *Engineering Geology, 201*, 96–105. https://doi.org/10.1016/j.enggeo.2015.12.027

Shi, Y., & Wang, C. Y. (1986). Pore pressure generation in sedimentary basins: overloading versus aquathermal. *Journal of Geophysical Research: Solid Earth, 91*(B2), 2153–2162. https://doi.org/10.1029/JB091iB02p02153

Smart, B. G. D., Somerville, J. M., Edlman, K., & Jones, C. (2001). Stress sensitivity of fractured reservoirs. *Journal of petroleum science and engineering, 29*(1), 29–37. https://doi.org/10.1016/S0920-4105(00)00088-7

Song, C., & Elsworth, D. (2020). Microbially induced calcium carbonate plugging for enhanced oil recovery. *Geofluids, 2020*, 1–10. https://doi.org/10.1155/2020/5921789

Song, C., Elsworth, D., Jia, Y., & Lin, J. (2022). Permeable rock matrix sealed with microbially-induced calcium carbonate precipitation: Evolutions of mechanical behaviors and associated microstructure. *Engineering Geology, 304*, Article 106697. https://doi.org/10.1016/J.ENGGEO.2022.106697

Song, C., Elsworth, D., Zhi, S., & Wang, C. (2021). The influence of particle morphology on microbially induced CaCO3 clogging in granular media. *Marine Georesources & Geotechnology, 39*(1), 74–81. https://doi.org/10.1080/1064119X.2019.1677828

Song, C., Chen, Y., & Wang, J. (2020). Plugging high-permeability zones of oil reservoirs by microbially mediated calcium carbonate Precipitation. *ACS omega, 5*(24), 14376–14383. https://doi.org/10.1021/acsomega.0c00902

Song, C., Wang, C., Elsworth, D., & Zhi, S. (2022). Compressive strength of MICP-treated silica sand with different particle morphologies and gradings. *Geomicrobiology Journal, 39*(2), 148–154. https://doi.org/10.1080/01490451.2021.2020936

Tan, X. H., Li, X. P., Liu, J. Y., Zhang, L. H., & Fan, Z. (2015). Study of the effects of stress sensitivity on the permeability and porosity of fractal porous media. *Physics Letters A, 379*(39), 2458–2465. https://doi.org/10.1016/j.physleta.2015.06.025

Tobler, D. J., Minto, J. M., El Mountassir, G., Lunn, R. J., & Phoenix, V. R. (2018). Microscale analysis of fractured rock sealed with microbially induced CaCO3 precipitation: influence on hydraulic and mechanical performance. *Water Resources Research, 54*(10), 8295–8308. https://doi.org/10.1029/2018WR023032

Wang, K., Wu, S., & Chu, J. (2023). Mitigation of soil liquefaction using microbial technology: an overview. *Biogeotechnics*Article 100005. https://doi.org/10.1016/j.bgtech.2023.100005

Wang, Y., Konstantinou, C., Tang, S., & Chen, H. (2023). Applications of microbial-induced carbonate precipitation: A state-of-the-art review. *Biogeotechnics*Article 100008. https://doi.org/10.1016/J.BGTECH.2023.100008

Wu, C., Chu, J., Wu, S., & Hong, Y. (2019). 3D characterization of microbially induced carbonate precipitation in rock fracture and the resulted permeability reduction. *Engineering Geology, 249*, 23–30. https://doi.org/10.1016/j.enggeo.2018.12.017

Zhang, Y., Hu, X., Wang, Y., & Jiang, N. (2023). A critical review of biomineralization in environmental geotechnics: Applications, trends, and perspectives. *Biogeotechnics*Article 100003. https://doi.org/10.1016/j.bgtech.2023.100003